PHYSICAL CHEMISTRY

Relativistic collapse of the classical triple bond in the CBi^- molecular ion

Deniz Kahraman[1]†, Jie Hui[1]†, Xin-Yu Zhang[1], Neil A. Ellis[1], Hyun Wook Choi[1]‡, Kirk A. Peterson[2]*, Lai-Sheng Wang[1]*

The conventional framework for chemical bonding between main-group elements involves separate σ and π orbitals to describe multiple bonds. However, relativistic effects mix these orbitals in molecules containing heavy elements through spin–orbit coupling, leaving the total angular-momentum projection (ω) as the only good quantum number. Direct experimental evidence that relativistic effects change the σ-π bonding framework has remained elusive. Here, we probe the carbon-bismuth triple bond in the CBi^- anion using high-resolution cryogenic photoelectron spectroscopy, coupled with relativistic four-component Dirac-Coulomb coupled-cluster calculations. Even though the CBi^- anion is isovalent to the well-known CN^- species, we demonstrate that the traditional σ + 2π triple-bond picture collapses into a pure π-like $|\omega| = 3/2$ and two $|\omega| = 1/2$ Kramers pairs containing substantial σ/π mixing.

The conventional concept of chemical bonding is founded on simultaneous conservation of orbital symmetry and electron spin. Emerging from Lewis's shared-electron model (*1*) and formalized by Pauling through solutions of the Schrödinger equation (*2*), this framework treats chemical bonding in terms of distinct spatial orbital symmetries. In the nonrelativistic limit, multiple bonds between main-group atoms are described by linear combinations of atomic orbitals that generate the familiar sigma (σ) and pi (π) orbitals, with electron spin retained as a separate quantum degree of freedom. This strict separation between orbital angular momentum and spin has underpinned our understanding of main-group bonding for nearly a century. Yet this separation is not fundamental; it is a consequence of the nonrelativistic approximation.

Although Pauling's picture (*2*) remains highly successful for light elements, it can fail for molecules containing heavy elements at the bottom of the periodic table, where spin–orbit coupling (SOC) becomes dominant. Over the past several decades, it has become clear that relativistic effects are not merely small spectroscopic corrections but fundamental determinants of chemical behavior in heavy-element molecules (*3*–*8*). Effects such as valence s- and p-orbital contraction and spin–orbit splitting reshape bond lengths, molecular geometries, thermodynamic stabilities, and chemical reactivity. Indeed, theoretical studies have shown that the chemistry at the bottom of the periodic table is governed to a large extent by relativity, whereas high-level bonding analyses have revealed that SOC can substantially modify the covalent character and electron density of heavy-element bonds beyond chemical intuition (*9*).

The Dirac equation fundamentally transformed the quantum-mechanical description of the electron (*10*) and many-electron systems (*11*). In the fully relativistic regime, especially near a heavy nucleus, the nonrelativistic picture breaks down. Most profoundly, strong SOC prevents the independent conservation of orbital and spin angular momenta. Under the Dirac Hamiltonian, spatial and spin degrees of freedom are intrinsically coupled, leaving the total angular-momentum projection (ω) as the relevant conserved quantity. In the traditional σ + 2π picture of a main-group triple bond, six electrons are distributed among orbitals with $m_l = 0, \pm1$ and $m_s = \pm1/2$. In the relativistic limit, however, each electron is described by a spinor with a single conserved projection, $\omega = m_l + m_s$, taking values of ±3/2 or ±1/2. Spinors with the same $|\omega|$ form Kramers pairs, the relativistic counterparts of orbitals (*12*). Because the conventional σ and π manifolds both generate spinors with $|\omega| = 1/2$, they share the same relativistic symmetry and are therefore allowed to interact and mix. Through this interaction, the corresponding Kramers pairs exchange orbital character, yielding bonding states that can depart drastically from the well-known σ and π framework (*13*, *14*). The observable chemical and physical consequences of this symmetry-driven mixing, however, have remained elusive.

To directly probe the transition from the nonrelativistic bonding picture, where spin and angular momentum are conserved separately, to a relativistic framework in which electrons pair according to their total angular momentum, we investigated the carbon–bismuth triple bond by photoelectron spectroscopy (PES) of the closed-shell CBi^- diatomic species. CBi^- is isovalent to the well-known triply bonded CN^- molecule, which conforms to the σ + 2π bonding picture. Bismuth, a heavy main-group element with 83 protons, provides an exceptionally relativistic environment, whereas the C–Bi diatomic unit offers a structurally simple platform in which relativistic effects can be isolated without the steric and electronic complications of larger systems. Using high-resolution cryogenic PES together with photoelectron angular distributions (PADs), we mapped the electronic structure of CBi^- and the vibrational profiles of the corresponding neutral radical with high precision. To interpret the experimental observations, we carried out fully relativistic four-component Dirac-Coulomb (DC) coupled-cluster calculations. This combined approach allows us to directly visualize how the σ and π molecular orbitals (MOs) reorganize into total-angular-momentum eigenstates under a relativistic framework. Beyond its conceptual importance, the Bi–C bond is also of growing importance in modern synthetic chemistry (*15*–*18*) because the properties of organobismuth compounds are fundamentally governed by their underlying electronic structure. The relativistic bonding concepts established here provide an essential framework for understanding Bi–C bonding in larger organobismuth systems and for rationalizing their emerging chemical behavior.

Photoelectron spectroscopy of the CBi^- anion

We generated the CBi^- anion by pulsed laser ablation of a cold-pressed Bi/graphite target (see materials and methods for details) in a supersonic cluster source. To probe the full valence electronic structure, we first obtained photoelectron spectra using a time-of-flight magnetic-bottle spectrometer (see materials and methods for experimental details) at photon energies of 3.496 eV (Fig. 1A) and 4.661 eV (Fig. 1B). The 4.661-eV spectrum exhibits three well-resolved electronic bands (X, A, and B), corresponding to detachment from the ground state of CBi^- to the ground state and the first two excited states of neutral CBi. A spectrum measured at 6.424 eV revealed no additional features (fig. S1). The lower-energy 3.496-eV spectrum affords higher resolution for the X and A bands and resolves their distinct Franck-Condon (FC) vibrational structure.

To fully resolve the vibrational structure in each detachment channel, we carried out high-resolution photoelectron imaging of cryogenically cooled CBi^- at 2.8114 eV for bands X and A (Fig. 1C), 3.9739 eV for band B (Fig. 1D), and 2.6212 eV for band X (fig. S2) (see materials and methods for experimental details). The resulting PADs are particularly valuable because they encode the angular-momentum character of the detachment orbital and the outgoing electron. Cryogenic cooling removed vibrational hot bands, allowing unambiguous assignment of the vibrational features in each electronic band. The binding

[1]Department of Chemistry, Brown University, Providence, RI, USA. [2]Department of Chemistry, Washington State University, Pullman, WA, USA. ***Corresponding author. Email: kipeters@wsu.edu (K.A.P.); lai-sheng_wang@brown.edu (L.-S.W.)** †These authors contributed equally to this work. ‡Present address: Sterling Chemistry Laboratory, Department of Chemistry, Yale University, New Haven, CT, USA.

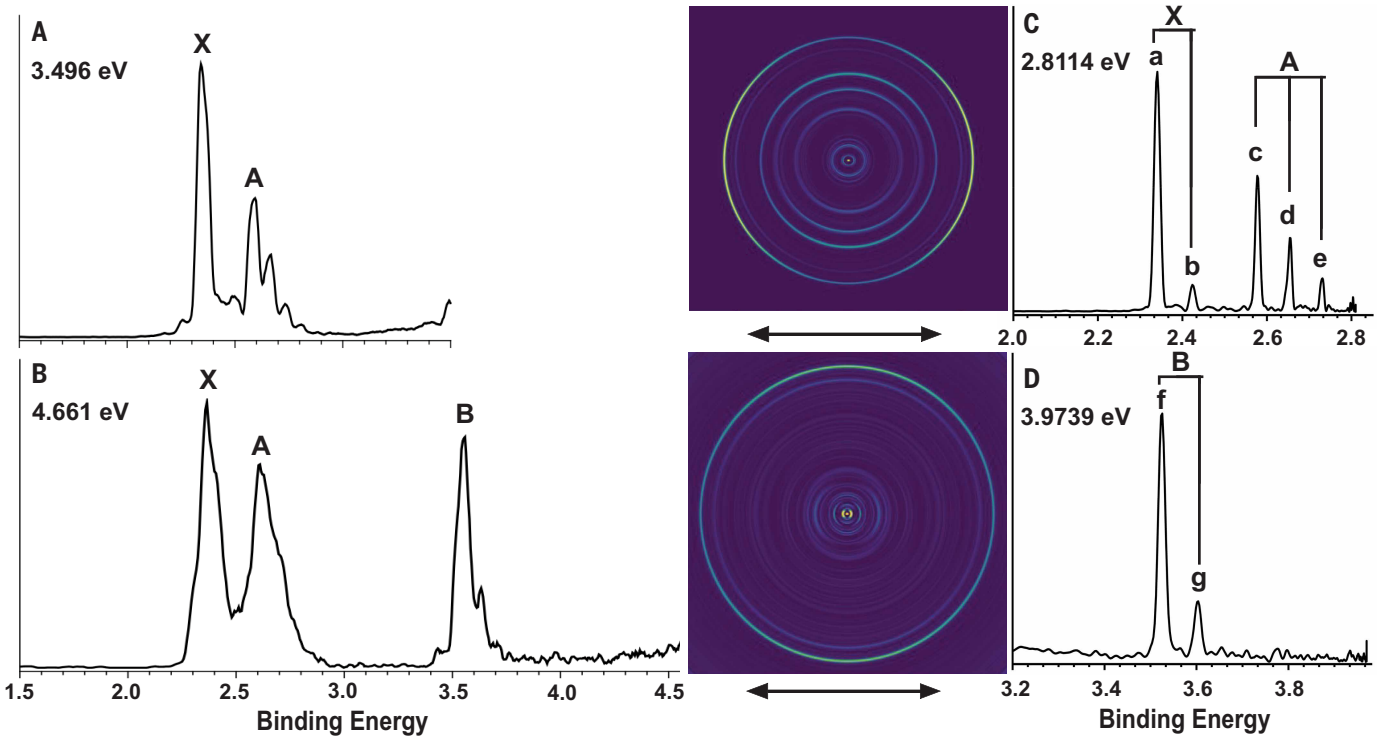

Fig. 1. Photoelectron spectroscopy and imaging of CBi^-. Photoelectron spectra were measured at (**A**) 3.496-eV and (**B**) 4.661-eV photon energies with a magnetic-bottle apparatus. High-resolution photoelectron imaging was done at (**C**) 2.8114-eV and (**D**) 3.9739-eV photon energies with cryogenically cooled CBi^- anions.

Table 1. The observed adiabatic detachment energies (ADE) for the CBi^- anion and the vibrational frequencies for the neutral final states in comparison with the corresponding theoretical results. The measured term values (T_e) for the first two excited states of CBi and the experimental photoelectron anisotropy parameter (β) for the three photodetachment transitions of CBi^- are also given.

Observed bands	Assignment	ADE (eV) (Exp.)*†	T_e (eV) (Exp.)*	ν (cm^{-1}) (Exp.)*	β (Exp.)‡	ADE (eV) (Theo.)§	ν (cm^{-1}) (Theo.)¶
X	$^2\Sigma^+$ ($\Omega = 1/2$)	2.3429	—	681	1.86	2.359	683
A	$^2\Pi$ ($\Omega = 3/2$)	2.5812	0.2383	606	−0.73	2.594	606
B	$^2\Pi$ ($\Omega = 1/2$)	3.5246	1.1817	633	−0.67	3.536	732

*Experimental uncertainty is ±0.0010 eV or ±8 cm^{-1}.
†The ADE and VDE (vertical detachment energy) are the same for all detachment channels.
‡For the X and A states, the β values were measured from the 2.8114-eV spectrum (Fig. 1C), and those for the B state were measured from the 3.9739-eV spectrum (Fig. 1D).
§DC-CCSD(T)/CBS (complete basis set) ADE includes contributions from the Gaunt interaction.
¶These include effects due to vibrational anharmonicity.

energies of all resolved vibrational peaks are summarized in table S1, and the spectroscopic information obtained is given in Table 1 in comparison with the theoretical results. The adiabatic detachment energies (ADEs), determined from the 0–0 transitions of bands X, A, and B, are 2.3429, 2.5812, and 3.5246 eV, respectively. Because the 0–0 transition is also the most intense FC feature in each band, these ADEs effectively match the corresponding vertical detachment energies (VDEs). The ADE of band X defines the electron affinity of CBi as 2.3429 eV. The high-resolution photoelectron imaging data also provide accurate vibrational frequencies of 681, 606, and 633 cm^{-1} for the X, A, and B states, respectively.

The vibrational frequencies and FC profiles of the detachment bands offer direct insight into the C–Bi bond in CBi^-. In the conventional bonding picture, the three PES bands would arise from electron detachment from the σ and π bonding orbitals of the closed-shell electron configuration ($\sigma^2\pi^4$) of CBi^- (Fig. 2, left). Detachment of a bonding electron would weaken the chemical bonds in the neutral final states, resulting in lower vibrational frequencies, longer equilibrium bond lengths, and broader FC progressions. Detachment from the σ MO would produce a $^2\Sigma^+_{1/2}$ final state, whereas detachment from the π MO would yield a $^2\Pi$ state split by SOC into $^2\Pi_{3/2}$ and $^2\Pi_{1/2}$. In the nonrelativistic regime, the two spin–orbit components would be expected to have similar bonding properties and hence similar FC profiles, as found for the isovalent CN^- and CO molecules (*19*, *20*). Instead, the present spectra show that the ground state (X) and the second excited state (B) have similarly short FC progressions dominated by their 0–0 transitions (peaks a and f), whereas the first excited state (A) displays a much more extended vibrational progression (peaks c, d, and e). This pronounced difference implies that the detachment orbitals leading to X and B have closely related bonding character, whereas the orbital giving rise to band A influences the C–Bi bond in a fundamentally different way.

However, the PADs extracted from the photoelectron images are incompatible with the nonrelativistic chemical-bonding picture. Quantified by the anisotropy parameter (β) (see materials and methods), the PADs provide a direct probe of the symmetry of the detachment orbital. The PAD of band X at 2.8114 eV (outermost ring in Fig. 1C)

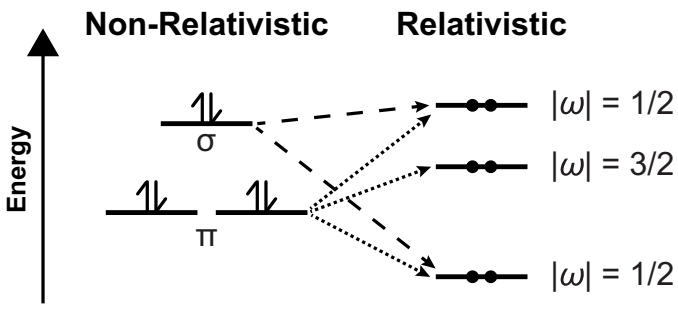

Fig. 2. Energy-level correlation diagram of the valence electrons of CBi^-. The transition from the nonrelativistic MO framework (left) to the fully relativistic Kramers pairs (right) is illustrated schematically. In the conventional picture (left), the arrows denote spin-up and spin-down electrons. Relativistically, SOC invalidates spin as a quantum number, so electrons are instead described by spinors forming Kramers pairs (depicted as dots). Dashed and dotted arrows indicate σ-type and π-type contributions to these pairs, respectively.

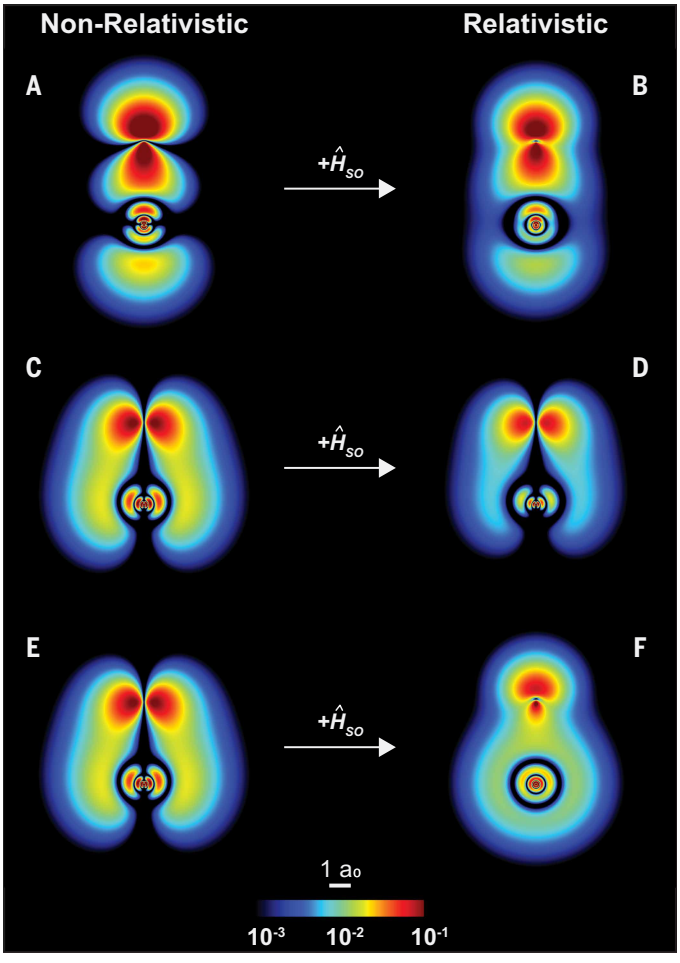

Fig. 3. Spin-orbit–induced transformation of the valence electron densities in CBi^-. The left column shows the nonrelativistic valence electron densities; the right column displays the corresponding fully relativistic electron densities under the influence of strong spin–orbit effects. The nonrelativistic σ orbital (**A**) turns into a mixed $|\omega| = 1/2$ Kramers pair (**B**); one π orbital (**C**) turns into a pure $|\omega| = 3/2$ Kramers pair (**D**); and the orthogonal degenerate π orbital (**E**) turns into a second mixed $|\omega| = 1/2$ Kramers pair (**F**). The molecular axis is oriented vertically, with the carbon atom positioned at the top and the bismuth atom positioned at the bottom.

displays a dominant p-wave behavior, with $\beta = 1.86$, indicating detachment from a σ-type orbital. By contrast, the PADs for band A (inner rings in Fig. 1C) and band B (Fig. 1D) show mixed s + d partial-wave behaviors, with $\beta = -0.73$ and -0.67, respectively, consistent with detachment from π-like orbitals. In the nonrelativistic framework, this PAD-based interpretation would lead to the assignments of band X to $^2\Sigma^+_{1/2}$ and bands A and B to the $^2\Pi_{3/2}$ and $^2\Pi_{1/2}$ states, respectively. Such an assignment, however, leads to a fundamental contradiction: The two spin–orbit components of the $^2\Pi$ manifold would have drastically different bonding properties, whereas the $^2\Sigma^+_{1/2}$ and $^2\Pi_{1/2}$ states would instead appear to have similar bonding characters.

To resolve this anomaly, the nonrelativistic bonding picture must be replaced by a fully relativistic one based on four-component DC calculations. In bismuth-containing systems, the SOC effect is so strong that the separation of spin and orbital angular momentum no longer holds, and the familiar σ and π MO concepts cease to be valid descriptors for CBi^-. To understand the experimental detachment bands qualitatively, we correlate the conventional picture with the fully relativistic scheme shown in Fig. 2, as outlined in the introduction. In the nonrelativistic limit, the triple bond in CBi^- consists of one σ and two degenerate π orbitals, giving rise to the closed-shell $\sigma^2\pi^4$ configuration, familiar in the isovalent CN^- and CO molecules. In the relativistic regime, however, only the total angular momentum $|\omega|$ remains conserved. The nominal π MO splits into $|\omega| = 1/2$ and 3/2 Kramers pairs, and the two $|\omega| = 1/2$ states can undergo symmetry-allowed mixing, as schematically shown in Fig. 2. As a result, the traditional triple bond is reorganized into three Kramers pairs in CBi^-. The strong mixing of the two $|\omega| = 1/2$ pairs accounts for the intermediate bonding behavior observed for band B, which lies between the predominantly σ character of the upper $|\omega| = 1/2$ pair (resulting in band X) and the pure π character of the $|\omega| = 3/2$ pair (resulting in band A). The PADs are particularly important in establishing the π-parentage of both the $|\omega| = 3/2$ pair and the $|\omega| = 1/2$ pair associated with band B. This interpretation is borne out completely by the four-component DC calculations.

Electronic structure calculations

To establish the structural basis of CBi^-, we computed the ground-state potential energy curve at the DC coupled cluster singles and doubles with perturbative triples [DC-CCSD(T)] level and obtained an equilibrium C–Bi bond length of 2.022 Å. Electron detachments were then evaluated by high-level coupled-cluster methods: The ADEs for the ground state (X) and the first excited state (A) were calculated at the DC-CCSD(T) level, whereas the ADE for the second excited state (B) was computed with the equation-of-motion ionization potential CCSD (EOM-IP-CCSD) method. To ensure quantitative accuracy, we used all-electron basis sets with deep electron correlation for all calculations. As shown in Table 1, the resulting four-component DC ADEs agree excellently with the experiment, supporting the conclusion that strong mixing between the two $|\omega| = 1/2$ Kramers pairs is the origin of the observed spectroscopic anomalies.

We also computed the anharmonic vibrational frequency of CBi^- (695 cm^{-1}) and those of the neutral final states (Table 1). The frequencies for the X and A states of CBi at the DC-CCSD(T) level of theory agree very well with the experimental values. The vibrational frequencies of the first two neutral states are lower than that of the anion, consistent with the bonding nature of the three Kramers pairs forming the triple bond in CBi^-. In the lighter isovalent CN or CO^+, the two SOC components ($^2\Pi_{3/2}$ and $^2\Pi_{1/2}$) have nearly identical potential energy curves and therefore similar vibrational frequencies and equilibrium bond lengths (*19*, *20*). Here, however, the B state [$^2\Pi(\Omega = 1/2)$] has a substantially higher frequency than the A state [$^2\Pi(\Omega = 3/2)$], a direct consequence of the strong mixing between the two $|\omega| = 1/2$ states. The relatively poor agreement between the EOM-IP-CCSD result and the experiment for the B state frequency suggests that this quantity is very sensitive to the degree of mixing between the X and B states,

although it is not clear why this mixing so strongly affects the B state frequency but not the frequency of the X state; the EOM-IP-CCSD frequencies for the X and A states are within about 8 cm^{-1} of the CCSD(T) results (see table S2). The PADs reinforce this mixing picture: The slightly smaller magnitude of the anisotropy parameter for B ($|\beta| = 0.67$), relative to A ($|\beta| = 0.73$), reflects admixture with the ground state. The clearest manifestation of this relativistic mixing is the FC structure: The FC profile of the B state becomes similar to that of X, whereas in the photoelectron spectra of CN^- or CO, the two SOC components exhibit identical FC profiles (*19*, *20*).

The different bonding characters of the three Kramers pairs and the consequences of relativistic mixing can be visualized directly in the two-dimensional spatial electron densities in Fig. 3. In the nonrelativistic picture, the σ orbital (Fig. 3A) and the doubly degenerate π orbitals (Fig. 3, C and E) are readily identified, although their densities are strongly polarized toward carbon. In the relativistic regime, however, the conventional σ + 2π description collapses. The $|\omega| = 3/2$ Kramers pair (Fig. 3D) still retains clear π character, but the two $|\omega| = 1/2$ Kramers pairs mix strongly, removing the π-like nodal plane from the lower $|\omega| = 1/2$ state (Fig. 3F). These electron density maps thus demonstrate vividly how the traditional triple bond between two lighter main-group atoms is transformed into the new relativistic triple bond in CBi^-, consisting of two mixed $|\omega| = 1/2$ Kramers pairs and a pure $|\omega| = 3/2$ Kramers pair.

Conclusions

High-resolution PES combined with fully relativistic four-component DC calculations provides clear evidence of the breakdown of the established triple-bond picture in the CBi^- diatomic system. The present results show that relativity can fundamentally reshape a textbook bonding paradigm even in a simple diatomic molecule. Whereas the light CN^- or related species are well described by the conventional σ + 2π triple bond, the photoelectron spectra and angular distributions of CBi^- expose strong mixing between the nominal $^2\Sigma^+_{1/2}$ and $^2\Pi_{1/2}$ states. This finding provides direct experimental evidence that strong SOC disrupts the conventional separation of σ and π bonding. The CBi^- species provides a benchmark system for probing how relativistic effects redefine multiple bonding in heavy-element molecules. More broadly, the present findings extend our understanding of the chemistry and physics of heavy elements and may have implications for the rational design of topological quantum materials, sustainable catalysis, and advanced actinide materials.

REFERENCES AND NOTES

1. G. N. Lewis, *J. Am. Chem. Soc.* **38**, 762–785 (1916).
2. L. Pauling, *J. Am. Chem. Soc.* **53**, 1367–1400 (1931).
3. P. Pyykkö, *Chem. Rev.* **88**, 563–594 (1988).
4. P. Pyykkö, *Annu. Rev. Phys. Chem.* **63**, 45–64 (2012).
5. P. Schwerdtfeger, M. Dolg, W. H. E. Schwarz, G. A. Bowmaker, P. D. W. Boyd, *J. Chem. Phys.* **91**, 1762–1774 (1989).
6. J. Autschbach, *J. Chem. Phys.* **136**, 150902 (2012).
7. K. S. Pitzer, *Acc. Chem. Res.* **12**, 271–276 (1979).
8. P. Pyykkö, J.-P. Desclaux, *Acc. Chem. Res.* **12**, 276–281 (1979).
9. T. Saue, *Chemphyschem* **12**, 3077–3094 (2011).
10. P. A. M. Dirac, *Proc. R. Soc. Lond., A Contain. Pap. Math. Phys. Character* **117**, 610–624 (1928).
11. P. A. M. Dirac, *Proc. R. Soc. Lond., A Contain. Pap. Math. Phys. Character* **123**, 714–733 (1929).
12. K. G. Dyall, K. Fægri Jr., *Introduction to Relativistic Quantum Chemistry* (Oxford Univ. Press, 2007).
13. P. A. Christiansen, K. S. Pitzer, *J. Chem. Phys.* **74**, 1162–1165 (1981).
14. K. Balasubramanian, *J. Phys. Chem.* **93**, 6585–6596 (1989).
15. N. M. Leonard, L. C. Wieland, R. S. Mohan, *Tetrahedron* **58**, 8373–8397 (2002).
16. T. Ollevier, *Org. Biomol. Chem.* **11**, 2740–2755 (2013).
17. O. Planas, F. Wang, M. Leutzsch, J. Cornella, *Science* **367**, 313–317 (2020).
18. Y. Pang, M. Leutzsch, N. Nöthling, J. Cornella, *J. Am. Chem. Soc.* **142**, 19473–19479 (2020).
19. S. E. Bradforth, E. H. Kim, D. W. Arnold, D. M. Neumark, *J. Chem. Phys.* **98**, 800–810 (1993).
20. J. E. Pollard, *Photoelectron Photoion Molecular Beam Spectroscopy* (Ph.D. thesis, Department of Chemistry, University of California, Berkeley, Berkeley, CA, 1982), p. 55.
21. D. Kahraman *et al.*, Tabular Data and Computational Details for the CBi Spectroscopic Analysis [Data set], Zenodo (2026); https://doi.org/10.5281/zenodo.20249312.

ACKNOWLEDGMENTS

We thank the Center for Computation and Visualization (CCV) at Brown University for assistance with part of the calculations. **Funding:** This work was funded by the National Science Foundation (grant no. CHE-2403841 to L.-S.W.). and the US Department of Energy (DOE), Office of Science, Office of Basic Energy Sciences, Heavy Element Chemistry Program (grant no. DE-SC0008501 to K.A.P.). **Author contributions:** Conceptualization: D.K., K.A.P., L.-S.W.; Methodology: D.K., J.H., H.W.C., K.A.P., L.-S.W.; Investigation: D.K., J.H., X.-Y.Z., N.A.E., H.W.C., K.A.P., L.-S.W.; Visualization: D.K., J.H.; Funding acquisition: K.A.P., L.-S.W.; Project administration: L.-S.W.; Supervision: K.A.P., L.-S.W.; Writing – original draft: D.K., L.-S.W.; Writing – review and editing: J.H., K.A.P. **Competing interests:** The authors declare that they have no competing interests. **Data, code, and materials availability:** Tabular data and four-component relativistic quantum chemical calculations have been deposited in Zenodo (*21*).

SUPPLEMENTARY MATERIALS

science.org/doi/10.1126/science.aei1285
Materials and Methods; Figs. S1 and S2; Tables S1 and S2; References (*22*–*35*)

Submitted 17 April 2026; accepted 19 May 2026

10.1126/science.aei1285

Relativistic collapse of the classical triple bond in the CBi# molecular ion

Deniz Kahraman, Jie Hui, Xin-Yu Zhang, Neil A. Ellis, Hyun Wook Choi, Kirk A. Peterson, and Lai-Sheng Wang

Science **393** (6807), . DOI: 10.1126/science.aei1285

Editor's summary

One of the most useful paradigms in chemistry is the distinction between sigma bonding symmetry along the bond axis and pi symmetry perpendicular to it. The cyanide ion, CN#, for instance, has one sigma and two pi bonds. It's long been clear that this model starts to fray when the atoms get heavy enough for relativity to come into play, but discrete observations have been lacking. Kahraman *et al*. now report photoelectron spectra and simulations of the bonding in the CBi# ion, where bismuth replaces nitrogen. The relativistic effects stemming from the massive bismuth mix the sigma and pi symmetries into an entirely different framework. —Jake S. Yeston